

ARTICLE

Received 12 Oct 2013 | Accepted 30 Dec 2013 | Published 27 Jan 2014

DOI: 10.1038/ncomms4185

Interaction of bipolaron with the $\text{H}_2\text{O}/\text{O}_2$ redox couple causes current hysteresis in organic thin-film transistors

Minni Qu¹, Hui Li¹, Ran Liu¹, Shi-Li Zhang^{1,2} & Zhi-Jun Qiu¹

Hysteresis in the current-voltage characteristics is one of the major obstacles to the implementation of organic thin-film transistors in large-area integrated circuits. The hysteresis has been correlated either extrinsically to various charge-trapping/transfer mechanisms arising from gate dielectrics or surrounding ambience or intrinsically to the polaron-bipolaron reaction in low-mobility conjugated polymer thin-film transistors. However, a comprehensive understanding essential for developing viable solutions to eliminate hysteresis is yet to be established. By embedding carbon nanotubes in the polymer-based conduction channel of various lengths, here we show that the bipolaron formation/recombination combined with the $\text{H}_2\text{O}/\text{O}_2$ electrochemical reaction is responsible for the hysteresis in organic thin-film transistors. The bipolaron-induced hysteresis is a thermally activated process with an apparent activation energy of 0.29 eV for the bipolaron dissociation. This finding leads to a hysteresis model that is generally valid for thin-film transistors with both band transport and hopping conduction in semiconducting thin films.

¹State Key Lab of ASIC & System, School of Information Science and Technology and School of Microelectronics, Fudan University, Shanghai 200433, China.

²Solid-State Electronics, The Ångström Laboratory, Uppsala University, Box 534, Uppsala SE-751 21, Sweden. Correspondence and requests for materials should be addressed to Z.-J.Q. (email: zjqiu@fudan.edu.cn).

Research on organic thin-film transistors (OTFTs) has recently made significant technological progress^{1–7}. However, OTFTs are still inferior to their silicon counterparts in terms of reproducibility and long-term stability. When an OTFT operates with its gate voltage (V_g) sweeping forwardly (from on to off) and reversely (from off to on), a hysteretic behaviour of its current is frequently observed and the threshold voltage (V_{th}) becomes bias-dependent^{8,9}. Current hysteresis can be a consequence of a variety of causes that can be either of extrinsic character such as interface charge traps^{10–12}, bulk traps in gate dielectrics^{13–15}, ambient atmosphere^{16–18} or of intrinsic origin represented by the bipolaron formation of slow mobile charge carriers especially in conjugated polymers^{19–21}. For OTFTs with SiO₂ as gate insulator, silanols on the SiO₂ surface¹⁰ as well as ambient absorbates¹⁶ have been of particular concern. Chakrapani *et al.*²² proposed that *p*-doping of diamond under ambient conditions was due to electron extraction from diamond to the H₂O/O₂ redox couple. This electrochemistry model was successfully employed by Aguirre *et al.*²³ to correlate the current hysteresis observed in thin-film transistors (TFTs) with carbon nanotube networks (CNNs) as conduction channel to a reversible electrochemical charge transfer between CNN and the H₂O/O₂ redox couple, rather than the often discussed mechanism invoking the interaction of the single-walled carbon nanotubes (SWCNTs) with silanol groups present on the SiO₂ surface. Aguirre *et al.*²³ further suggested that the electrochemical effect should be ubiquitous and not limited to organic semiconductor devices.

The mobile charge carriers in low-mobility organic semiconductors are commonly modelled as polarons and their transport is usually limited by interchain hopping. Polarons at high concentrations can form doubly charged bipolarons^{19–21}. Bipolarons are immobile owing to an improbable two-carrier hopping at the same time. Thus, formation and subsequent dissociation of bipolarons prompted by V_g could cause current hysteresis in OTFTs. However, Coulomb repulsion between two positively charged polarons makes the bipolaron formation unfavourable. Counterions are essential in formation²⁴ and stabilization of bipolarons¹⁹. Thus far, the origin of counterions is unclear and has been assumed to be extrinsic dopants²⁵ or oxygen ions¹⁹. Therefore, the complex hysteresis phenomenon in OTFTs remains poorly understood despite extensive studies.

We embed SWCNTs in poly(9,9-dioctylfluorene-co-bithiophene) (F8T2), a conjugated polymer, to facilitate a systematic investigation of current hysteresis, as they represent two typical semiconducting materials with distinct transport mechanisms: hopping and band transport²⁶. Their hysteresis behaviour has

been studied, separately, using F8T2-capacitors²⁴ and CNN-TFTs²⁷. We show that by varying the channel length, L , of the composite-TFTs, the transport mechanism spans from SWCNT-dominating band transport along a percolating network to F8T2-dominating hopping on sub-percolating paths. The presence of SWCNTs in F8T2 can effectively reduce L in the sub-percolation regime, although the physical L is much longer²⁸. As a result, a significant current enhancement compared with having F8T2 alone in the channel is anticipated. In this report, we demonstrate that the hysteresis in OTFTs is caused by an interaction between bipolaron and the H₂O/O₂ redox couple. This finding leads to a comprehensive model for hysteresis generally valid for TFTs of both band transport and hopping conduction in semiconducting thin films.

Results

Device architecture and channel morphology. The schematic structure of a bottom-contact composite-TFT is shown in Fig. 1a. The TFT fabrication is detailed in Methods. The atomic force microscopy image of the composite film in Fig. 1b clearly indicates individual or small bundles of SWCNTs being sparsely embedded in the polymer host. Sharing a similar aromatic structure, the fluorene-based F8T2 strongly interact with and well disperse SWCNTs, thereby leading to a stable F8T2/SWCNT composite^{29,30}.

Electrical characterization. The typical transfer characteristics of *p*-type composite-TFTs for various L are depicted in Fig. 2a. Severe current hysteresis is evident and can be characterized by the difference in V_{th} for forward (V_{th}^f) and reverse (V_{th}^r) sweep. The threshold voltages, together with the hysteresis gap (defined as $\Delta V_{th} = V_{th}^f - V_{th}^r$), are found to be strongly dependent on L . As illustrated in Fig. 2b, V_{th}^f is around -12 V and almost independent of L , while V_{th}^r undergoes a continuous negative shift for $L > 60$ μm , resulting in an L -dependent ΔV_{th} . The distinct behaviour of V_{th}^f and V_{th}^r is discussed later.

As shown in Fig. 2c, the on-current (I_{on}) of the composite-TFTs decreases gradually with increasing L , while the off-current (I_{off}) experiences a step-like decline by almost two orders of magnitude at a critical channel length $L_C = 60$ μm . Thereafter, I_{off} remains fairly constant at ~ 10 pA. As a result, an I_{on}/I_{off} peak at $\sim 10^4$ appears at L_C . The abrupt decline of I_{off} (or the resulting sharp increase in I_{on}/I_{off}) is a signature of the breakdown of the percolating network²⁸ and the TFT device is now operated in the sub-percolating regime (Fig. 2d, inset). This experimental observation is verified by Monte Carlo simulation by

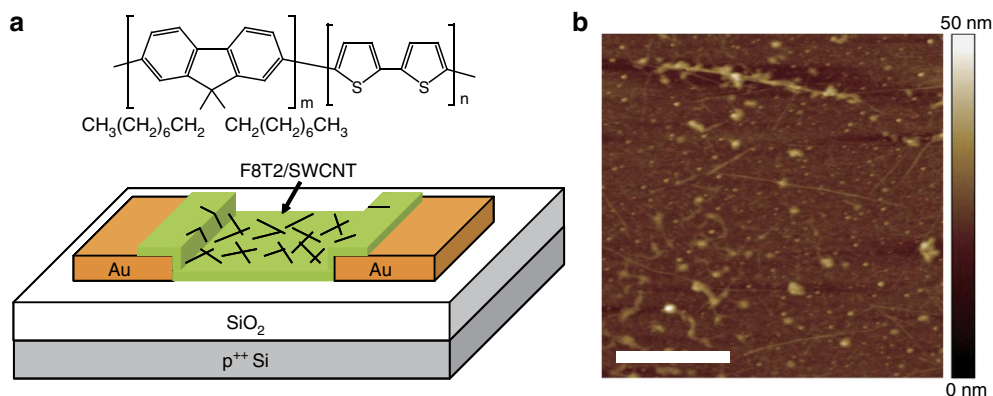


Figure 1 | Basic device structure. (a) Schematic structure of a back-gate TFT with an F8T2/SWCNT composite film, with the chemical structure of F8T2 shown in the inset. (b) Atomic force microscopy image in height mode of the conduction channel, with a low density of 6 SWCNTs per μm^2 dispersed in the F8T2 host. The scale bar in **b** is 1 μm .

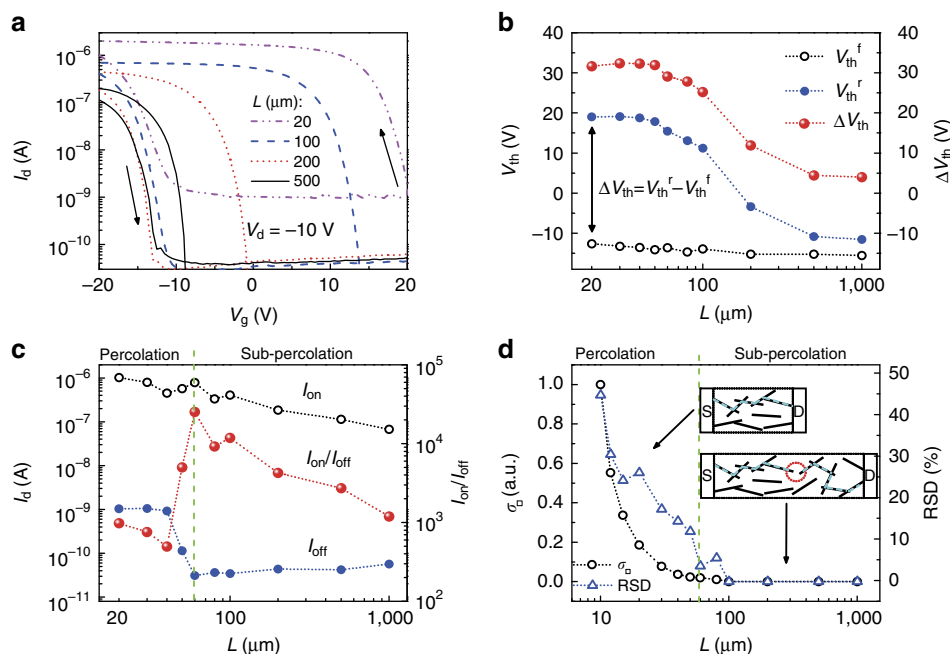
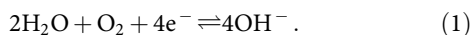


Figure 2 | Verification of distinct conduction mechanisms. (a) Transfer characteristics of composite-TFTs with various L , measured at $V_d = -10 \text{ V}$, with the black arrows indicating the V_g sweep directions. The channel width of the TFTs is fixed at $500 \mu\text{m}$. (b) Dependence of V_{th}^f and V_{th}^r as well as of ΔV_{th} on L for the TFTs in a. V_{th}^f and V_{th}^r are determined at the same I_d of 10 nA . (c) Variation of I_{on} and I_{off} and of I_{on}/I_{off} with L for the same TFTs. (d) Monte Carlo simulation of sheet conductance (σ_{\square}) and the relative s.d. versus L for a CNN conduction channel. Upper inset shows a percolating SWCNT network in a short channel with the cyan dashed line representing a percolation pathway. In the lower inset, the network no longer percolates in a long channel with the red dotted circle indicating the short break in the CNN that is linked by F8T2 in the composite-TFTs. The black arrows point to the corresponding conduction regimes. The green dashed lines at $L_C = 60 \mu\text{m}$ in c and d indicate the transition from percolation to sub-percolation as the dominant conduction mechanism.

representing the percolation probability³¹ with the normalized sheet conductance (σ_{\square}). The simultaneous fall of σ_{\square} and its relative s.d. to zero around $L_C = 60 \mu\text{m}$ in Fig. 2d suggests that the percolation path breaks altogether at this length. Here, the measured SWCNT density at $6 \mu\text{m}^{-2}$ is used as an input parameter in the simulation. With the composite, the non-zero conductance for $L > 60 \mu\text{m}$ in Fig. 2c is because of the sub-percolation conduction through the F8T2 host.

In the percolation regime, V_{th}^f and V_{th}^r are independent of L , resulting in a constant hysteresis gap, which is consistent with the results on CNN-TFTs^{14,17,32}. As shown by Aguirre *et al.*²³, the following electrochemical reaction is responsible for the hysteresis in CNN-TFTs:



Here, the electrochemical potential of the redox couple under the ambient conditions is about -5.3 eV , which lies near the top edge of the valence band of SWCNTs. The electron transfer from SWCNTs to the redox couple is then easy, which is the reason why SWCNTs and most organic semiconductors exposed to air are p -type. In the reverse sweep, the starting positive V_g pushes the $\text{H}_2\text{O}/\text{O}_2$ electrochemical potential further downward relative to that of SWCNTs. This would promote the electrons being transferred from SWCNTs to the $\text{H}_2\text{O}/\text{O}_2$ redox couple to form OH^- ions that lead to electrostatic screening of the gate field. In the forward sweep, however, the starting negative V_g drives the electrochemical reaction in equation (1) in the reverse direction. This leads to the consumption of OH^- ions. Consequently, the change in the amount of absorbed negative charges on the SWCNT surface during the forward and reverse sweeps produces the observed hysteresis. The magnitude of ΔV_{th} depends on the sweep range and rate^{17,27,32}.

Use of pulsed measurements with V_g pulses of alternating polarities, that is, the AP method, has been reported to distinctively reduce the hysteresis in CNN-TFTs compared with using continuous sweeping^{33,34}. As shown in Fig. 3a, the hysteresis of a composite-TFT of $L = 20 \mu\text{m}$ is almost completely eliminated using the AP method, confirming that the OH^- -induced excessive carriers during the positive V_g pulse are immediately removed by the subsequent negative pulse. All our devices operating in the percolation regime show hysteresis behaviour consistent with the previous work on CNN-TFTs³⁴⁻³⁷. In sharp contrast, the AP method causes little difference from the continuous sweeping regarding the hysteresis behaviour of long-channel devices ($L = 1,000 \mu\text{m}$) (Fig. 3b). In these devices, hopping conduction dominates in the sub-percolating F8T2/SWCNT composite. The electrochemical charge transfer occurring between F8T2 and the absorbed $\text{H}_2\text{O}/\text{O}_2$ redox couple is therefore predominating over that between SWCNTs and the redox couple. Different from the short-channel composite-TFTs, the channel of the long-channel devices remains in the off-state at $V_g = 0 \text{ V}$ for the reverse sweep, resulting in a smaller ΔV_{th} . The $\text{H}_2\text{O}/\text{O}_2$ electrochemistry theory alone cannot provide a satisfactory explanation to the hysteresis behaviour in the sub-percolation regime where F8T2 plays a predominating role in channel conduction. Concurrently, the bipolaron mechanism was proposed by Street *et al.*¹⁹ to explain the bias-stress effect and V_{th} shift in F8T2-TFTs. Immobile bipolarons are suggested to form at negative V_g in the reverse sweep during which polarons start to accumulate in the channel. At the beginning of the forward sweep, the bipolaron dissociation is retarded due to a large energy barrier. The retention of the bipolarons at the interface leads to a negative shift of V_{th} . Although the bipolaron mechanism can partly explain the

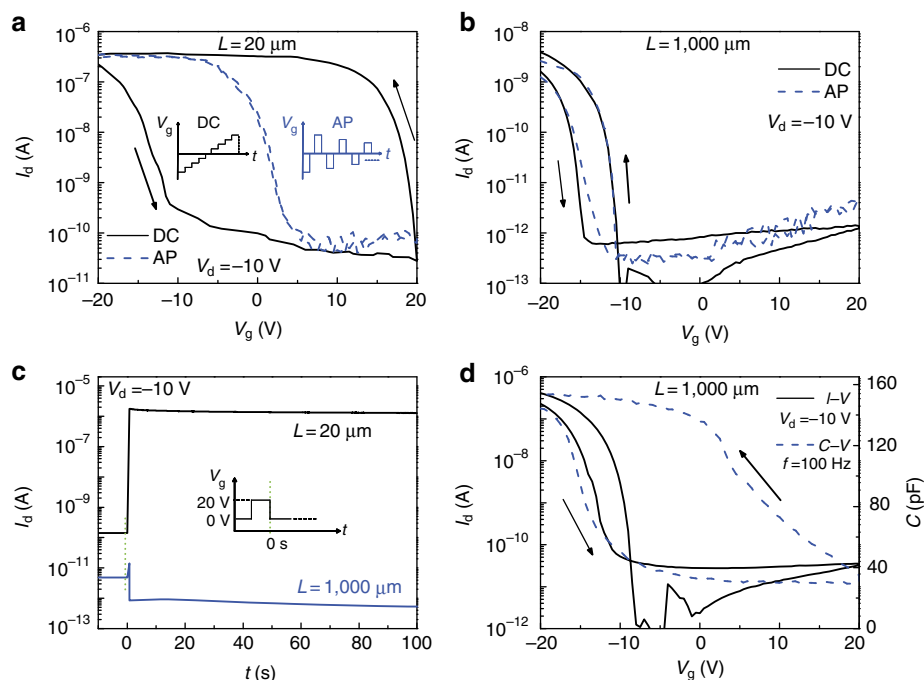
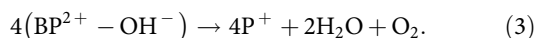
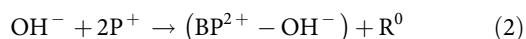


Figure 3 | Distinct hysteresis behaviour between percolating and sub-percolating devices. (a,b) Transfer characteristics of composite-TFTs with $L = 20 \mu\text{m}$ (a) and $L = 1,000 \mu\text{m}$ (b) with V_g sweeping in DC mode and AP mode. Inset in a schematically shows the DC and AP mode of V_g sweep. (c) Time dependence of I_d for the composite-TFTs of $L = 20 \mu\text{m}$ and $L = 1,000 \mu\text{m}$ in the first 100 s, in response to a single gate pulses of $V_g = 20 \text{ V}$ for 1 s (inset). The green dashed lines indicate the starting point of timing. (d) Forward and reverse V_g sweep of I - V and C - V curves of the composite-TFTs of $L = 1,000 \mu\text{m}$, at $V_d = -10 \text{ V}$ for I - V and frequency of 100 Hz for C - V , respectively.

observed hysteresis, it fails to interpret why I_{off} in the reverse sweep is lower than that in the forward sweep since I_{off} should be less affected by the bipolaron formation¹⁹. Moreover, the formation of bipolarons requires a high concentration of counterions, a critical point seldom discussed in the literature so far.

The $\text{BP}^{2+} - \text{OH}^-$ complex model. In what follows, a model that invokes the bipolaron formation/recombination in combination with the $\text{H}_2\text{O}/\text{O}_2$ electrochemical reaction is proposed to account for the distinct hysteresis behaviour in the sub-percolating composite-TFTs. The polaron-bipolaron equilibrium is represented in equation (2) for the formation of bipolaron-hydroxyl complex, denoted as the $\text{BP}^{2+} - \text{OH}^-$, and in equation (3) for its recombination:



Here, R^0 represents a neutral chain segment of F8T2 (ref. 24). In the sub-percolating composite-TFTs, electrons are transferred from the composite to the $\text{H}_2\text{O}/\text{O}_2$ redox couple at positive V_g and $\{\text{OH}^-\}$ s are electrochemically generated. The presence of OH^- induces polaron accumulation in F8T2 at positive V_g . More significantly, two positively charged polarons are, with the assistance of the negative charged OH^- , able to overcome the Coulomb repulsion and form the $\text{BP}^{2+} - \text{OH}^-$ complex. By transforming most polarons to the immobile $\text{BP}^{2+} - \text{OH}^-$ complex, a low drain current, I_d , is retained even at negative V_g . Recombination of the $\text{BP}^{2+} - \text{OH}^-$ complex under sufficiently large negative V_g , in accordance to equation (3), leads to release of mobile polarons and increase in I_d . This process contradicts Street's bipolaron theory in that it builds on bipolaron

dissociation rather than formation at negative V_g in the reverse sweep. In the forward sweep, V_{th}^f experiences a slight negative shift, due to the reduction of OH^- at negative V_g , leading to the observed hysteresis. Furthermore, I_{off} becomes higher than that in the reverse sweep as a result of the retarded bipolaron formation at positive V_g in the forward sweep. Therefore, by varying L of the composite-TFTs, the hysteresis mechanism changes from the $\text{H}_2\text{O}/\text{O}_2$ electrochemical reaction in the percolation regime to the polaron-bipolaron formation/recombination coupled to the $\text{H}_2\text{O}/\text{O}_2$ reaction in the sub-percolation regime. Specifically, V_{th} is governed by the polaron-bipolaron transition and $\text{H}_2\text{O}/\text{O}_2$ electrochemical process in the reverse sweep but is less affected in the forward sweep. This explains why V_{th}^f strongly varies with L while V_{th}^r largely remains constant.

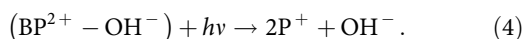
The distinct hysteresis behaviour between short-channel and long-channel composite-TFTs can be further demonstrated with a single-pulse measurement. A single positive gate bias pulse for 1 s was applied to two typical devices, one with $L = 20 \mu\text{m}$ and the other with $L = 1,000 \mu\text{m}$ (Fig. 3c). The positive gate pulse is applied to form an ample amount of OH^- . They are expected to decay after the pulse. For the shorter-channel device, the $\text{H}_2\text{O}/\text{O}_2$ electrochemical process induces holes in the percolating SWCNTs during positive gate pulse, resulting in an abrupt increase in I_d by four orders of magnitude followed by a slow decrease with the electrochemistry reaching equilibrium at zero gate voltage. As to the sub-percolating device of $L = 1,000 \mu\text{m}$, the conduction is dominated by hopping in the F8T2 host. The polaron production induced by the $\text{H}_2\text{O}/\text{O}_2$ redox couple at the positive gate pulse is quickly transformed to the immobile $\text{BP}^{2+} - \text{OH}^-$ complex, resulting in an almost fivefold reduction in I_{off} . These results confirm that the bipolaron formation occurs at positive V_g .

Although most of the polarons have transformed to immobile $\text{BP}^{2+} - \text{OH}^-$ having no contribution to I_d , any remaining

polarens can respond to capacitance–voltage (C – V) measurement and thus resulting in a different hysteresis behaviour. This hypothesis is verified in Fig. 3d, with the C – V and I – V measurements carried out on the same TFT. The C – V measurement was performed at low frequency to avoid the transmission line effect^{38,39}. The C – V flatband is almost identical to V_{th}^f in the forward sweep, as expected. The C – V flatband in the reverse sweep shifts farther than V_{th}^f to positive voltage, resulting in a wider capacitance hysteresis gap than ΔV_{th} . The positive flatband voltage shift confirms that the channel is not totally depleted of polarons and the remaining polarons are able to respond the AC small signal superimposed on the DC voltage during the C – V measurement.

Dissociation of the BP^{2+} – OH^- complex under illumination.

Like excitons in inorganic semiconductors, the BP^{2+} – OH^- complex is expected to dissociate under illumination according to:



Here, $h\nu$ is the energy of incident photons. As shown in Supplementary Fig. 1, V_{th}^f significantly shifts to more positive voltage while V_{th}^r is less affected during white-light illumination. Thus, a remarkable hysteresis gap comparable with that for the short-channel percolating devices is evident for the long-channel sub-percolating composite-TFTs. Light absorption by SWCNTs does not affect the hysteresis behaviour (Supplementary Fig. 2), while a reference F8T2-TFT shows a similar hysteresis behaviour to the long-channel sub-percolating composite-TFTs (Supplementary Fig. 3). Hence, the illumination helps dissociate almost all immobile BP^{2+} – OH^- complex formed at positive V_g in the reverse sweep into mobile polarons. Further, such illumination-induced hysteresis can be eliminated using the AP method, as for the short-channel devices.

The hysteresis behaviour is strongly dependent on the illumination wavelength, λ , as shown in Fig. 4a for the transfer characteristics at different wavelengths. The variation of ΔV_{th} with λ relative to ΔV_{th} in dark is plotted along with the optical absorption spectrum of an F8T2 film in Fig. 4b. The pristine F8T2 film shows a strong absorption in the visible range with two local peaks around 460 and 480 nm, corresponding, respectively, to the π – π^* transitions on the F8T2 backbone⁴⁰. The variation of ΔV_{th} with λ correlates well to the absorption spectrum, suggesting that the conduction carriers in the long-channel composite-TFTs in the reverse sweep not only arise from the dissociation of the BP^{2+} – OH^- complex, but also from the free carriers and excitons created by the bandgap light adsorption. Beyond the absorption edge of the F8T2 film, the small increase in ΔV_{th} is also evident for those at 545 and 578 nm where the F8T2 absorption is negligible. In this beyond-bandgap absorption region, the increase in ΔV_{th} is obviously mainly caused by the dissociation of the BP^{2+} – OH^- complex.

In order to further investigate the effects of beyond-bandgap light illumination, a near-infrared laser at 785 nm is used. The transfer characteristics under the 785-nm illumination with relative laser power density, P , are shown in Fig. 4c, yielding a well-correlated relation $\Delta V_{th} \propto P^{1/4}$ (Fig. 4d). This relationship is understood as follows. Variation of ΔV_{th} is equivalent to the shift in V_{th}^f . The latter is affected by the variation of polaron density in F8T2, N_p , and follows the relation⁴¹, $\Delta V_{th} \propto N_p^{1/2}$. The change in bipolaron density is found to be proportional to the square of the polaron concentration¹⁹, $\Delta N_{BP} \propto N_p^2$. With reference to equation (4), ΔN_{BP} should be proportional to the number of incident photons or the laser power density, hence, $\Delta N_{BP} \propto P$. These relationships finally yield the experimentally found $\Delta V_{th} \propto P^{1/4}$ in Fig. 4d and Supplementary Fig. 4 for 633-nm illumination. Finally, the light induced increase in ΔV_{th} beyond the F8T2 bandgap is attributed to the dissociation of the BP^{2+} – OH^- complex by postulating that the photon energy

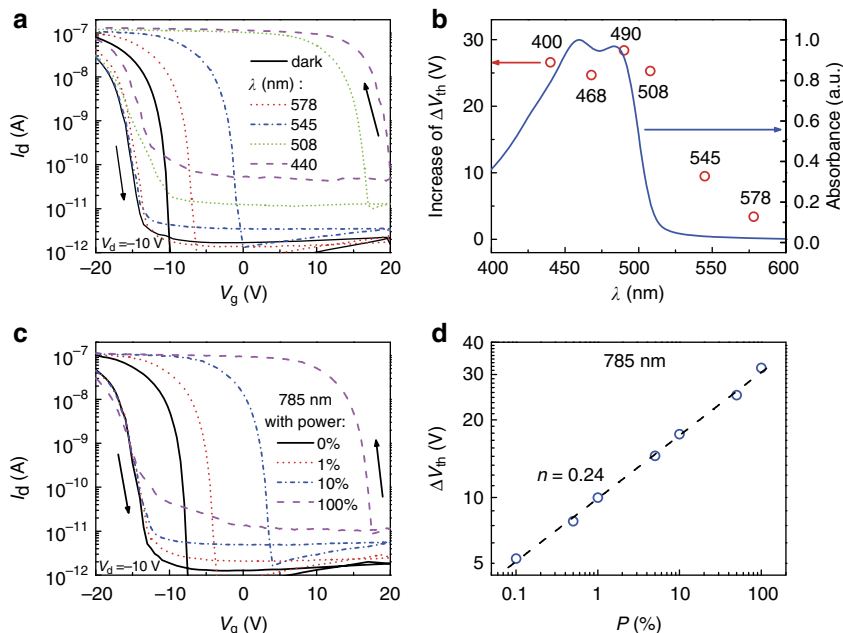


Figure 4 | Optical response of sub-percolating composite-TFTs of $L = 1,000 \mu\text{m}$. (a) Typical transfer characteristics measured in darkness and under illumination at different wavelengths. (b) Optical response in terms of increase in ΔV_{th} at several wavelengths of illumination from 400–600 nm (red circles) for the TFT in a. For comparison, the blue solid curve shows the absorption spectrum of an F8T2 polymer thin film. (c) Typical transfer characteristics measured in darkness and under the illumination at 785 nm wavelength with increasing laser power density P (relative). (d) ΔV_{th} (blue circles) versus P in log–log scale for the TFT in c. The linear fitting in the log–log scale (black dashed line) shows that ΔV_{th} increases with P following a power function with the index $n = 0.24$.

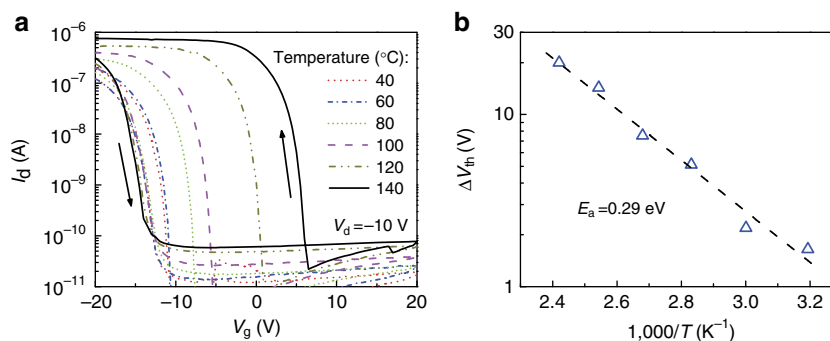


Figure 5 | Temperature response of sub-percolating composite-TFTs of $L = 1,000 \mu\text{m}$. (a) Evolution of transfer characteristics with measurement temperature. (b) Arrhenius representation of ΔV_{th} versus reciprocal absolute temperature (blue triangles). The linear fitting in log-linear scale (black dashed line) shows that the process of ΔV_{th} development is a thermally activated one with an apparent activation energy of 0.29 eV.

1.58 eV for the 785-nm laser is larger than the binding energy of the complex. The hysteresis behaviour is thus a thermally activated process for the long-channel sub-percolating composite-TFTs.

Thermal activation energy of the $\text{BP}^{2+}\text{-OH}^-$ complex. The temperature dependence of ΔV_{th} for the long-channel devices is shown in Fig. 5a. When presented in an Arrhenius plot in Fig. 5b, the mathematical equivalence $\Delta V_{\text{th}} \propto \exp(-E_a/k_B T)$ is well followed by all experimental data. Here, E_a is the apparent activation energy for the dissociation of the complex, k_B the Boltzmann constant, and T the absolute temperature. Further, such thermally-induced hysteresis can be eliminated by characterizing the devices at elevated temperatures, for example, 140 °C, in combination with using the AP method (Supplementary Fig. 5). A good linear fit of the data points in Fig. 5b gives $E_a = 0.29 \text{ eV}$. According to Street *et al.*¹⁹, the formation energy of bipolarons would be larger than 0.2 eV for a significant bipolaron concentration at room temperature while it should be above 0.5 eV to completely convert holes to bipolarons. The binding energy of the $\text{BP}^{2+}\text{-OH}^-$ complex depends on the structure order of the polymer. The regioregular form of conjugated polymers has smaller bipolaron binding energies, which is attributed to the delocalization of the holes arising from the π - π stacking in the two-dimensional structure of the ordered lamellae. The strong π - π interaction between F8T2 and SWCNTs would assist the F8T2 polymer chains to align in parallel with SWCNTs, thereby increasing the polymer conjugation length^{42,43}. The longer conjugation length, the smaller is the bipolaron binding energy. Hence, use of composite-TFTs is more advantageous in clarifying the origin of hysteresis than using pristine F8T2-TFTs.

Discussion

In conclusion, a generic model for current hysteresis in TFTs is proposed. By employing a composite semiconductor comprising SWCNTs embedded in F8T2 films as the conduction channel, we are able to design a unique series of TFTs with channel lengths varying by 2 orders of magnitude in order to confirm the origin of hysteresis in OTFTs. For short-channel devices where the SWCNTs percolate in the conduction channel, the hysteresis behaviour resembles that in CNT-FETs and CNN-TFTs, that is, it is caused by the $\text{H}_2\text{O}/\text{O}_2$ electrochemical process interacting with the SWCNTs. Consequently, the hysteresis gap ΔV_{th} is independent of channel length, light illumination and measurement temperature. For long-channel devices in which electronic hopping in the F8T2 matrix prevails for current conduction, the

origin of hysteresis is identified to be the formation/dissociation of bipolarons triggered by the $\text{H}_2\text{O}/\text{O}_2$ redox reaction. Contrary to the bipolaron mechanism discussed in the literature, the bipolaron is formed at the off-state instead of the on-state and manifests itself in the $\text{BP}^{2+}\text{-OH}^-$ complex. The bipolaron-induced hysteresis is sensitive to light illumination even with the beyond-bandgap light. It is also a thermally activated process, with an apparent activation energy of 0.29 eV extracted for the dissociation of the $\text{BP}^{2+}\text{-OH}^-$ complex. The established model provides useful guidelines for a deep understanding of hysteresis in TFTs.

Methods

Solution preparation. Both F8T2 (Sigma-Aldrich) and HiPco-SWCNTs (Unidym, average diameter 1.1 nm and average length 1.5 μm) were used as received. F8T2 was first dissolved into toluene (Sigma-Aldrich) in a sonic bath. SWCNTs were ultrasonically added into the F8T2/toluene solution (0.1 mg ml⁻¹) followed by centrifugation at 13,300 g for 60 min. The supernatant was then carefully decanted for the TFT fabrication and optical characterization. The ultraviolet-visible absorption spectrum of a thin-film F8T2 drop-cast on a quartz substrate was carried out with a Perkin-Elmer Lambda 750S spectrophotometer.

TFT fabrication. Heavily doped *p*-type Si wafers were used as the substrate and back gate, whereas a 100-nm SiO_2 was thermally grown as the gate dielectric. Source and drain electrodes comprising a 50-nm-thick Au layer on top of a 5-nm-thick Ti adhesion layer were defined by means of electron-beam evaporation followed by lift-off. The distance between the source/drain electrodes, that is, the channel length, was varied from 20–1,000 μm . The channel regions were then opened by lithography. For each experiment, one chip was sliced out of the wafer and thin films of F8T2 or F8T2/SWCNT composite were deposited by dip-coating the chip in the polymer solution for 12 h. The chip was then carefully pulled out and baked at 90 °C to remove the residual solvent. The film formed outside the channel was stripped off in acetone along with the photoresist. After blown-dry in N_2 , a 10-min hot-plate baking at 90 °C completed the device fabrication. All the processes were performed under ambient conditions. For the reference CNN-TFT, the chip fabrication was identical to the process described above and the SWCNT conduction channel was formed by dip-coating the chip in the SWCNT/surfactant solution.

Device characterization. A Keithley 4200 semiconductor characterization system and Agilent 4284A precision LCR metre were utilized for *I*-*V* and *C*-*V* measurements of the TFTs, respectively. The temperature-varying *I*-*V* characterization was performed with a Temptronic temperature controller. All characterizations were usually carried out in dark except for illumination experiments. The illumination experiments were performed at room temperature with a Halogen lamp (12 V, 100 W) filtered through 20-nm-bandpass filters on a Leica microscope (DM2500 M). The optical density of each filtered wavelength was measured with a calibrated Si photodiode (440 nm: 34.2 $\mu\text{W cm}^{-2}$, 468 nm: 119 $\mu\text{W cm}^{-2}$, 490 nm: 68.3 $\mu\text{W cm}^{-2}$, 508 nm: 92.3 $\mu\text{W cm}^{-2}$, 545 nm: 141 $\mu\text{W cm}^{-2}$, 578 nm: 103 $\mu\text{W cm}^{-2}$). For long-wavelength illuminations, a 17-mW 633-nm He-Ne laser and 250-mW 785-nm near-infrared diode laser were used with various attenuators to reduce the laser intensity.

References

- Crone, B. *et al.* Large-scale complementary integrated circuits based on organic transistors. *Nature* **403**, 521–523 (2000).
- Dimitrakopoulos, C. D. & Malenfant, P. R. L. Organic thin film transistors for large area electronics. *Adv. Mater.* **14**, 99–117 (2002).
- Gelinck, G. H. *et al.* Flexible active-matrix displays and shift registers based on solution-processed organic transistors. *Nat. Mater.* **3**, 106–110 (2004).
- Yan, H. *et al.* A high-mobility electron-transporting polymer for printed transistors. *Nature* **457**, 679–686 (2009).
- Sekitani, T., Zschieschang, U., Klauk, H. & Someya, T. Flexible organic transistors and circuits with extreme bending stability. *Nat. Mater.* **9**, 1015–1022 (2010).
- Jung, M. *et al.* All-printed and roll-to-roll-printable 13.56-MHz-operated 1-bit RF tag on plastic foils. *IEEE Trans. Elec. Dev.* **57**, 571–580 (2010).
- Di, C.-A., Zhang, F. & Zhu, D. Multi-functional integration of organic field-effect transistors (OFETs): advances and perspectives. *Adv. Mater.* **25**, 313–330 (2013).
- Egginger, M., Bauer, S., Schwödiauer, R., Neugebauer, H. & Sariciftci, N. S. Current versus gate voltage hysteresis in organic field effect transistors. *Monatsh. Chem.* **140**, 735–750 (2009).
- Bobbert, P. A., Sharma, A., Mathijssen, S. G. J., Kemerink, M. & de Leeuw, D. M. Operational stability of organic field-effect transistors. *Adv. Mater.* **24**, 1146–1158 (2012).
- Chua, L.-L. *et al.* General observation of n-type field-effect behaviour in organic semiconductors. *Nature* **434**, 194–199 (2005).
- Lee, J. S. *et al.* Origin of gate hysteresis in carbon nanotube field-effect transistors. *J. Phys. Chem. C* **111**, 12504–12507 (2007).
- Hiraoka, M., Yamada, T. & Hasegawa, T. Bias stress and condensation of mobile trap agents in printed organic transistors. *Appl. Phys. Lett.* **95**, 223304 (2009).
- Singh, T. B. *et al.* High-performance ambipolar pentacene organic field-effect transistors on poly(vinyl alcohol) organic gate dielectric. *Adv. Mater.* **17**, 2315–2320 (2005).
- Fuhrer, M. S., Kim, B. M., Dürkop, T. & Brintlinger, T. High-mobility nanotube transistor memory. *Nano Lett.* **2**, 755–759 (2002).
- Radosavljević, M., Freitag, M., Thadani, K. V. & Johnson, A. T. Nonvolatile molecular memory elements based on ambipolar nanotube field effect transistors. *Nano Lett.* **2**, 761–764 (2002).
- Gu, G. & Kane, M. G. Moisture induced electron traps and hysteresis in pentacene-based organic thin-film transistors. *Appl. Phys. Lett.* **92**, 053305 (2008).
- Kim, W. *et al.* Hysteresis caused by water molecules in carbon nanotube field-effect transistors. *Nano Lett.* **3**, 193–198 (2003).
- Choi, H. H., Lee, W. H. & Cho, K. Bias-stress-induced charge trapping at polymer chain ends of polymer gate-dielectrics in organic transistors. *Adv. Funct. Mater.* **22**, 4833–4839 (2012).
- Street, R. A., Salleo, A. & Chabiny, M. L. Bipolaron mechanism for bias-stress effects in polymer transistors. *Phys. Rev. B* **68**, 085316 (2003).
- Salleo, A. & Street, R. A. Kinetics of bias stress and bipolaron formation in polythiophene. *Phys. Rev. B* **70**, 235324 (2004).
- Paasch, G. Transport and reactions in doped conjugated polymers: electrochemical processes and organic devices. *J. Electroanal. Chem.* **600**, 131–141 (2007).
- Chakrapani, V. *et al.* Charge transfer equilibria between diamond and an aqueous oxygen electrochemical redox couple. *Science* **318**, 1424–1430 (2007).
- Aguirre, C. M. *et al.* The role of the oxygen/water redox couple in suppressing electron conduction in field-effect transistors. *Adv. Mater.* **21**, 3087–3091 (2009).
- Paasch, G., Scheinert, S., Herasimovich, A., Hörselmann, I. & Lindner, T. h. Characteristics and mechanisms of hysteresis in polymer field-effect transistors. *Phys. Stat. Sol. A* **205**, 534–548 (2008).
- Paasch, G. Transport in doped conjugated polymers with polarons and bipolarons forming complexes with counter ions. *Solid State Ionics* **169**, 87–94 (2004).
- Coropceanu, V. *et al.* Charge transport in organic semiconductors. *Chem. Rev.* **107**, 926–952 (2007).
- Jin, S. H. *et al.* Sources of hysteresis in carbon nanotube field-effect transistors and their elimination via methylsiloxane encapsulants and optimized growth procedures. *Adv. Funct. Mater.* **22**, 2276–2284 (2012).
- Bo, X.-Z. *et al.* Carbon nanotubes-semiconductor networks for organic electronics: the pickup stick transistor. *Appl. Phys. Lett.* **86**, 182102 (2005).
- Nish, A., Hwang, J.-Y., Doig, J. & Nicholas, R. J. Highly selective dispersion of single-walled carbon nanotubes using aromatic polymers. *Nat. Nanotech.* **2**, 640–646 (2007).
- Liu, Z., Li, H., Qiu, Z., Zhang, S.-L. & Zhang, Z.-B. Small-hysteresis thin-film transistors achieved by facile dip-coating of nanotube/polymer composite. *Adv. Mater.* **24**, 3633–3638 (2012).
- Li, J., Zhang, Z.-B. & Zhang, S.-L. Percolation in random networks of heterogeneous nanotubes. *Appl. Phys. Lett.* **91**, 253127 (2007).
- Vijayaraghavan, A. *et al.* Charge-injection-induced dynamic screening and origin of hysteresis in field-modulated transport in single-wall carbon nanotubes. *Appl. Phys. Lett.* **89**, 162108 (2006).
- Mattmann, M. *et al.* Pulsed gate sweep strategies for hysteresis reduction in carbon nanotube transistors for low concentration NO₂ gas detection. *Nanotechnology* **21**, 185501 (2010).
- Liu, Z., Qiu, Z.-J., Zhang, Z.-B., Zheng, L.-R. & Zhang, S.-L. Mobility extraction for nanotube TFTs. *IEEE Elec. Dev. Lett.* **32**, 913–915 (2011).
- Lin, H. & Tiwari, S. Localized charge trapping due to adsorption in nanotube field-effect transistor and its field-mediated transport. *Appl. Phys. Lett.* **89**, 073507 (2006).
- Mattmann, M., Bechstein, D., Roman, C., Chikkadi, K. & Hierold, C. Reduction of gate hysteresis above ambient temperature via ambipolar pulsed gate sweeps in carbon nanotube field effect transistors for sensor applications. *Appl. Phys. Lett.* **97**, 153103 (2010).
- Estrada, D., Dutta, S., Liao, A. & Pop, E. Reduction of hysteresis for carbon nanotube mobility measurements using pulsed characterization. *Nanotechnology* **21**, 085702 (2010).
- Esen, G., Fuhrer, M. S., Ishigami, M. & Williams, E. D. Transmission line impedance of carbon nanotube thin films for chemical sensing. *Appl. Phys. Lett.* **90**, 123510 (2007).
- Liu, Z. *et al.* On gate capacitance of nanotube networks. *IEEE Elec. Dev. Lett.* **32**, 641–643 (2011).
- Levermore, P. A., Jin, R., Wang, X., de Mello, J. C. & Bradley, D. D. C. Organic light-emitting diodes based on poly(9,9-dioctylfluorene-co-bithiophene) (F8T2). *Adv. Funct. Mater.* **19**, 950–957 (2009).
- Sze, S. M. & Ng, K. K. *Physics of Semiconductor Devices*. Ch. 4 (Wiley, 2007).
- Chen, J. *et al.* Noncovalent engineering of carbon nanotube surfaces by rigid, functional conjugated polymers. *J. Am. Chem. Soc.* **124**, 9034–9035 (2002).
- Zou, J. *et al.* Dispersion of pristine carbon nanotubes using conjugated block copolymers. *Adv. Mater.* **20**, 2055–2060 (2008).

Acknowledgements

This work is supported partially by the National Natural Science Foundation of China (Nos. 61204090 and 61171010), Shanghai Municipal Natural Science Foundation (No. 12ZR1402700), Cultivation Fund of the Key Scientific and Technical Innovation Project, Ministry of Education of China (No. 708033), Special Funds for Major State Basic Research Projects of China (No. 2011CBA00603), Fundamental Research Project of young teachers to enhance research capacity, Fudan University (No. 20520133248) and Swedish Research Council (VR) (No. 2009-8068).

Author contributions

Z.-J.Q. and M.Q. conceived and designed the experiments. M.Q. and H.L. carried out solution preparation and TFT fabrication. M.Q. performed atomic force microscopy, electrical and optical measurements. H.L. and Z.-J.Q. performed numerical simulation. M.Q., Z.-J.Q. and S.-L.Z. wrote the manuscript. All authors discussed the results and revised the manuscript. S.-L.Z. directed the project.

Additional information

Supplementary Information accompanies this paper at <http://www.nature.com/naturecommunications>

Competing financial interests: The authors declare no competing financial interests.

Reprints and permission information is available online at <http://npg.nature.com/reprintsandpermissions/>

How to cite this article: Qu, M. *et al.* Interaction of bipolaron with the H₂O/O₂ redox couple causes current hysteresis in organic thin-film transistors. *Nat. Commun.* **5**:3185 doi: 10.1038/ncomms4185 (2014).